



Insights into the electrode reaction process of nickel nanoparticles @reduced graphene oxide catalyst for ethanol oxidation in alkaline solution

Xiaoguang Li^{1,2} · Sashuang Ning² · Xiaoya Liu² · Enbo Shangguan² · Chengke Wu² · Jing Li² · Zhenhui Wang² · Quanmin Li²

Received: 4 January 2019 / Revised: 19 February 2019 / Accepted: 25 February 2019 / Published online: 22 March 2019

© Springer-Verlag GmbH Germany, part of Springer Nature 2019

Abstract

Nickel nanoparticles uniformly anchored on reduced graphene oxide (Ni/RGO) nanosheets is successfully prepared by a facile wet-chemical method. It is found that many small Ni nanoparticles with the particle size of 4–8 nm are anchored on RGO, showing uniform dispersion. The Ni/RGO nanocomposite-modified glassy carbon electrode (GCE) (i.e., Ni/RGO/GCE) is investigated as an electrocatalyst for the ethanol oxidation reaction. Especially, the as-prepared Ni/RGO/GCE delivers excellent electrocatalytic performance in terms of the low peak potential value, the low reduction of its overvoltage, and satisfactory peak current density. The excellent electrocatalytic properties could be ascribed to the synergistic effect of Ni spherical nanoparticles and RGO nanosheets, which can lead to the high use ratio of Ni. It is proposed that the anodic peak that emerged in the potential negative-going sweep may be attributed to the oxidation of ethanol, which results from the high concentration of ethanol and an autocatalytic process at Ni/RGO/GCE.

Keywords Ethanol oxidation · Nickel nanoparticles · Reduced graphene oxide · Catalyst

Introduction

In recent years, direct ethanol fuel cells (DEFCs) have received considerable attention owing to their high energy density and conversion efficiency, low operating temperature, and environmental friendliness [1–7]. Especially, compared with methanol and formic acid, ethanol possesses numerous advantages of higher theoretical mass energy density, non-toxic, low

cost, and availability [2, 4]. Furthermore, it can be produced in large quantity by the fermentation process of sugar-containing biomass or agricultural products [2]. As a result, DEFCs as alternative power sources have achieved increasing interest in their application in the fields of automobile and portable consumer electronics [8, 9]. However, before the commercialization of DEFCs, several challenges should be solved, one of which is to develop an electrocatalyst with a high activity and a competitive price. As is well known, Pt and Pt-based catalysts are considered as promising and most effective catalysts in DEFCs and have been intensively studied for many years [4, 10–16]. However, Pt catalysts still suffer from multiple problems such as slow reaction kinetics, high cost, poor durability, etc. [2, 4]. Though massive research has been conducted to reduce the amount of Pt [4, 10–16], the expensive cost and limited reserve of Pt catalysts significantly hinder its application in DEFCs. Therefore, it would be highly incentive to develop efficient, durable, and inexpensive alternatives to substitute Pt-based catalysts.

Nickel and nickel-based nanocomposites, as less expensive analogs of platinum, have been recognized as effective electrocatalysts for the direct oxidation of small organic

✉ Xiaoguang Li
lxg819@126.com

✉ Jing Li
lijing8825@163.com

¹ School of Chemistry and Chemical Engineering, Xinxiang University, Xinxiang 453003, People's Republic of China

² Collaborative Innovation Center of Henan Province for Green Manufacturing of Fine Chemicals, Key Laboratory of Green Chemical Media and Reactions, Ministry of Education, School of Chemistry and Chemical Engineering, Henan Normal University, Xinxiang 453007, People's Republic of China

molecules [2, 5, 17–20]. Many studies have demonstrated that nickel can deliver a high activity for electrooxidation of alcohol in alkaline media, confirming an attractive and effective candidate to be applied as an electrocatalyst for the ethanol oxidation reaction [21]. It is also reported that for a small organic molecule, the catalytic oxidation processes generated by the Ni-based materials are attributed to the formation of a high-valent, oxyhydroxide species [NiOOH] in alkaline medium [17]. As we know, catalyst support with superior electrical conductivity, high surface area, and chemical stability plays a great role on the catalytic activity improvement. In general, using a proper carbon-based support to anchor nanocatalysts is considered as another effective strategy for the enhancement of their catalytic properties for ethanol oxidation [4, 12, 22–27]. Owing to their higher electrical conductivity, excellent mechanical as well as their high specific surface area, graphene and its derivatives have been extensively applied as a good support for catalysts and electrode materials [2, 4, 28–30].

Recently, many types of nickel-based nanocomposites have been proposed as electrocatalysts for the ethanol oxidation in alkaline solution, such as Ni/activated hydrothermal carbon composite [23], nano-Ni/graphite [24], Ni-based alloy [31], mesoporous nickel/nickel hydroxide [32], NiCo/NRGO prepared by nitrogen-doped reduced graphene oxide (RGO) with NiCo nanoparticles [33], Ni-MW-NP/CPE fabricated using carbon paste electrode (CPE) modified by nanoporous nickel phosphate molecular sieves and multiwalled carbon nanotubes (MWCNT) [34], polycrystalline nickel electrode [35], MWCNT/Ni catalysts [36], Ni/graphene aerogel [37], N-doped carbon-encapsulated nickel nanoparticles [38], and NiCo/C-N/CNT composite [39], as well as Ni/NA/MWCNT/Ch/WGE constructed by nickel nanoparticles, 4-nitroaniline (NA), MWCNT, choline (Ch), graphite [40], etc. Nevertheless, there is still a lot of room to enhance its electrocatalytic property. To the best of our knowledge, electrocatalytic properties of reduced graphene oxide-supported nickel nanoparticles (Ni/RGO) for ethanol oxidation in alkaline solution have rarely been studied and remain largely unknown. In addition, the action mechanism and electrode process of nickel-based electrocatalyst for ethanol oxidation reaction in an alkaline medium are not yet adequately understood [23, 24]. In this context, the objectives of this study are to fabricate a Ni/RGO nanocomposite by a facile method and to evaluate its electrocatalytic properties, and further to explore its electrode reaction process for ethanol oxidation.

In this paper, Ni/RGO nanosheets have been fabricated through a facile, low-cost, and environmentally friendly route by reducing nickel salt and GO with NaBH₄. In this nanocomposite, nickel nanoparticles are uniformly deposited on the surface of RGO, showing good dispersibility. The Ni/RGO nanocomposite-modified glassy carbon electrode (GCE) (i.e., Ni/RGO/GCE) is investigated as an electrocatalyst for

the ethanol oxidation reaction for fuel cells using cyclic voltammetry and chronoamperometry. Especially, in comparison to some previous work, the as-prepared Ni/RGO nanosheet electrode displays a better catalytic role for ethanol oxidation in terms of the lower peak potential value and the reduction of its overvoltage. It is discovered that the as-prepared Ni/RGO/GCE delivers excellent electrocatalytic performance due to the synergistic effect of small Ni spherical nanoparticles and RGO nanosheets.

Experimental section

Materials

Graphite powder (99.95%) and H₂O₂ (30%) were purchased from Shanghai Sinopharm Chemical Reagent Co., Ltd. (Shanghai, China). Ethanol and NaBH₄ were obtained from Chemical Reagent Co., Ltd. of Shantou and Beijing, respectively. All the other chemicals were of analytical grade and used without further purification. All the aqueous solutions were prepared with twice-distilled water in all of the experiments.

Preparation of the nickel/reduced graphene oxide (Ni/RGO)

In a typical procedure, graphene oxide (GO) was prepared from natural graphite powder using a modified Hummers method [40]. The Ni/RGO was prepared using a one-step reaction procedure. For preparing the Ni/RGO sheets, the theoretical molar ratios of the elements C, Ni, and B, which were originally from the flake graphite, NiSO₄·6H₂O, and NaBH₄ respectively, were controlled at 125:9:30. The concentration of the ultrasonically dispersed GO suspension was diluted to 9.0 mg mL⁻¹ with deionized water, and 6 mM of NiSO₄·6H₂O was dropwise added to the as-prepared suspension of graphene oxide sheets. The mixture was stirred for 2 h, and then the pH value was adjusted to 10.0 with the aqueous ammonia. Next, an aqueous NaBH₄ solution of 0.2 M with the desired mole number of B (NaBH₄) was trickled into the mixture. After reaction for 30 min, the Ni/RGO was formed and then filtered and washed using deionized water and alcohol sequentially.

Preparation of Ni/RGO/GCE

For the preparation of the Ni/RGO/GCE, 2 mg of Ni/RGO powder was dispersed into 1.0 mL water by ultrasonication for 20 min to obtain a homogeneous suspension. Then, 3 μL of the Ni/RGO suspension was dropped onto the surface of the pre-polished glassy carbon electrode (GCE, 0.3 cm in

diameter) and dried at room temperature. As a result, the Ni/RGO/GCE-modified electrode was fabricated.

Characterization

The structural information of the GO and Ni/RGO was obtained by X-ray diffraction (XRD) using a Bruker D8 X diffractometer with Cu K α radiation. Raman spectra of the GO and Ni/RGO were collected using a HR800 Raman spectrometer with a laser excitation energy of 532 nm. Scanning electron microscopy (SEM) was performed with an S-3400NII scanning electron microanalyzer with energy-dispersive X-ray spectrometry (EDS). Transmission electron microscopy (TEM) images were acquired using a JEM-2100 Ffield emission TEM at 200 kV, after dispersing the Ni/RGO nanohybrids in ethanol and depositing several drops of the suspension on the carbon-coated copper grids and drying them under ambient conditions. The loading content of Ni in the Ni/RGO nanohybrids was identified with an IRIS Advantage inductively coupled plasma atomic emission spectrometer (ICP-AES).

Electrochemical measurements

Electrochemical measurements were made on a CHI832 electrochemical workstation (CH Instruments, Chenhua Co., Shanghai, China). A conventional three-electrode system was used, containing a saturated calomel electrode (SCE) as the reference electrode, a Pt wire as the counter electrode, and the bare or modified glassy carbon electrodes (GCE) as the working electrode. The electrocatalytic activity of the Ni/RGO-modified electrode was examined by cyclic voltammetry in 1.0 M NaOH. To investigate the catalytic activity and mechanism of the Ni/RGO toward ethanol oxidation, cyclic voltammetric experiments, in 1.0 M NaOH containing 0.1 M ethanol or 0.1 M acetaldehyde saturated with N₂, were performed at a scan rate of 50 mV s⁻¹ with 0–0.6 V of potential scanning region.

Results and discussions

Material characterization

The typical FE-SEM images of the as-prepared GO and Ni/RGO nanosheets are illustrated in Fig. 1. As shown in Fig. 1a, b, the GO sample is composed of GO nanosheets with a curly and wavy morphology, which is beneficial to achieve a high surface area. FE-SEM images (Fig. 1c, d) of Ni/RGO display that the Ni/RGO remains a similar wrinkled surface morphology like GO. Especially, it can be seen that the Ni/RGO shows more pronounced wrinkles than GO and no agglomerate of Ni particles can be observed, indicating that Ni/RGO can easily

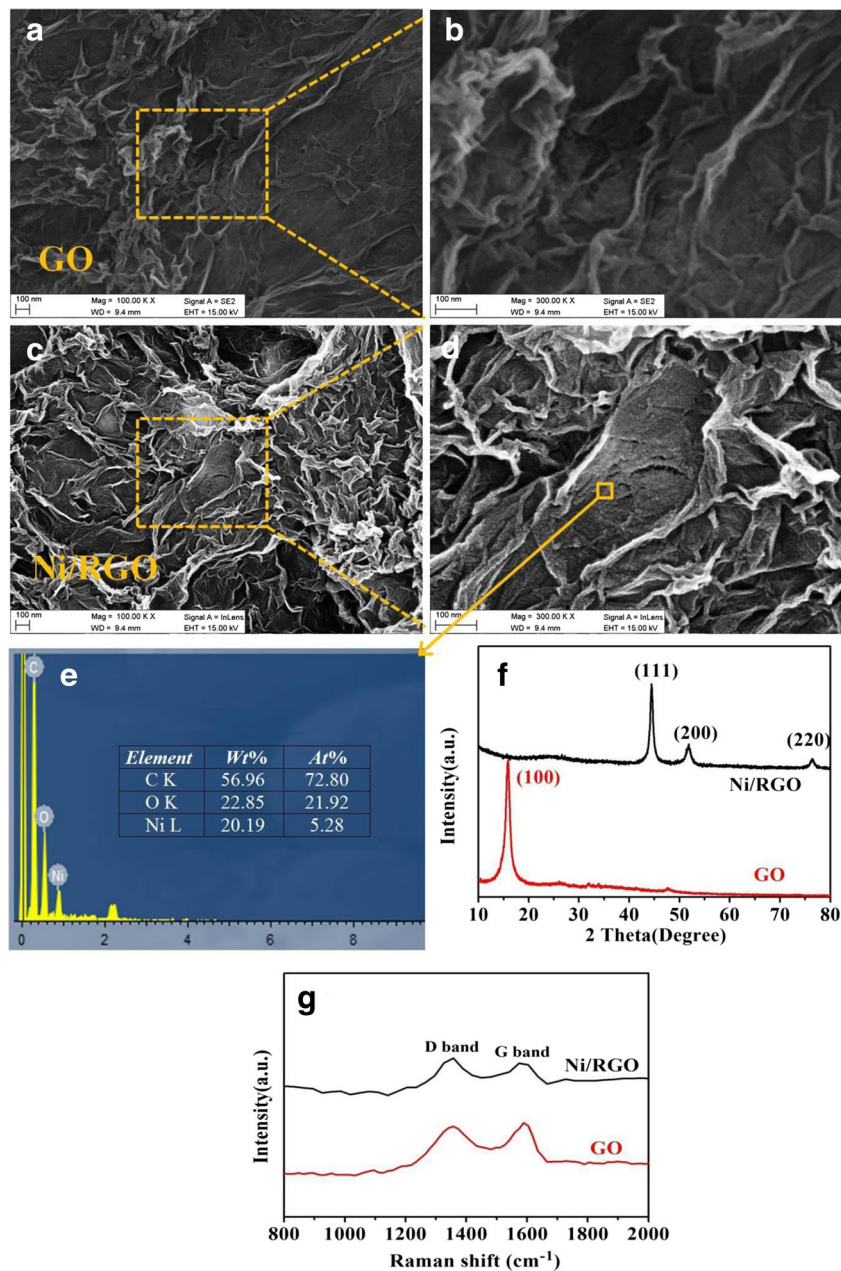
reserve high specific surface area and Ni nanoparticles were highly dispersed on the surface of RGO sheets. The EDS spectrum (Fig. 1e) shows that the obtained Ni/RGO nanosheets consist of three elements of nickel, carbon, and oxygen and no other impurity phases are detected. An ICP test shows that the loading content of nickel nanoparticles in the Ni/RGO nanosheets is 19.65%.

Figure 1f displays the typical XRD patterns of the GO and Ni/RGO nanosheets. It can be seen that the GO shows a strong peak centered at 10.2°, which is indexed to its (001) reflection. As for the Ni/RGO, three main peaks at 44.3°, 51.4°, and 76.3° are detected, which correspond to the (111), (200), and (220) diffraction planes of Ni (JCPDS No. 65-2865), respectively [30]. In addition, the characteristic peak of GO is not detected and a broad peak centered at 25° (the characteristic peak of RGO) is observed in the XRD pattern of Ni/RGO, illustrating that GO has been effectively reduced to RGO by NaHB₄. This result is further confirmed by the test of Raman spectrum, which has been generally conducted to characterize carbon and carbon-based materials. As shown in Fig. 1g, the GO and Ni/RGO show two characteristic peaks at about 1355 cm⁻¹ (D band) and 1590 cm⁻¹ (G band) [41]. Generally, the intensity ratio of the D band to the G band (I_D/I_G) plays a great role in the evaluation of the degree of crystallinity of the carbon materials. In this work, the value of I_D/I_G increases from 0.95 of the GO to 1.05 of the Ni/RGO nanocomposite, illustrating the enhancement of the crystallinity degree of the Ni/RGO. This is because some new and smaller sp² domains have formed through the reduction reaction and the loading of Ni nanoparticles [30, 41].

The microstructures of the GO and the Ni/RGO were further investigated using TEM and HRTEM, as shown in Fig. 2. It can be seen from Fig. 2a that the GO is substantially composed of thin nanosheets. From Fig. 2b, it can be clearly seen that nearly monodispersed Ni nanospheres are anchored uniformly on the surface of RGO nanosheets, showing an excellent dispersion. The higher magnification TEM image of Fig. 2c displays that the spherical nickel nanoparticles exhibit a diameter size of about 4–8 nm, which are almost separated from each other. Figure 2d shows the HRTEM image of Ni/RGO. It is obvious that the Ni nanospheres have an interplanar distance of about 0.21 nm, corresponding to the (111) plane of the crystallized Ni phase, confirming that the Ni/RGO nanohybrid has been successfully achieved [30, 41].

Figure 3 displays the XPS spectra of the Ni/RGO sample. The C1s spectrum of Ni/RGO (Fig. 3a) displayed the characteristic peaks of C=C, C–C (at 284.8 eV), C–O–H, C–O–C (at 286.7 eV), and O=C–OH (at 288.05 eV), confirming the presence of epoxide, hydroxyl, and carboxyl group. Figure 3b shows

Fig. 1 Low-magnification and high-magnification FE-SEM images of the as-prepared GO (a, b) and Ni/RGO nanohybrids (c, d); e EDX spectrum of Ni/RGO nanocomposite; f XRD patterns of GO and Ni/RGO nanocomposite



the Ni 2p spectrum. It is obviously seen that the Ni 2p_{3/2} can be identified into four peaks at 852.4, 855.4, 855.8, and 862.1 eV, respectively, corresponding to Ni(0), NiO, Ni(OH)₂, and the satellite peak [42]. This confirms the successful deposition of Ni nanoparticles on the surface of RGO, which is consistent with some previous reports [42, 43]. The existence of oxidized species of Ni suggests its low-degree oxidized surface, which is mainly due to the environment containing O₂ and H₂O [44]. Furthermore, as shown in Fig. 3c, the O1s spectrum shows that the peak located at 531.9 eV mainly results from the oxidized species of Ni and the residual oxygen-containing groups that bonded with C atoms in RGO [44].

Electrochemical measurements

Figure 4a shows the surface cyclic voltammograms (CVs) for the RGO/GCE and Ni/RGO/GCE in blank electrolyte (1.0 M NaOH) solution in the absence of ethanol. In the case of RGO/GCE (curve b in Fig. 4a), no obvious redox peaks are detected. In contrast, as for the Ni/RGO/GCE, a pair of well-defined redox peaks with an anodic peak at 0.405 V and a cathodic peak at 0.305 V are observed, which can correspond to the Ni(III)/(II) redox couple [17, 45]. According to some reported work, the redox peaks at the Ni/RGO/GCE were attributed to Ni(OH)₂/NiOOH shift reaction. According to literature [17],

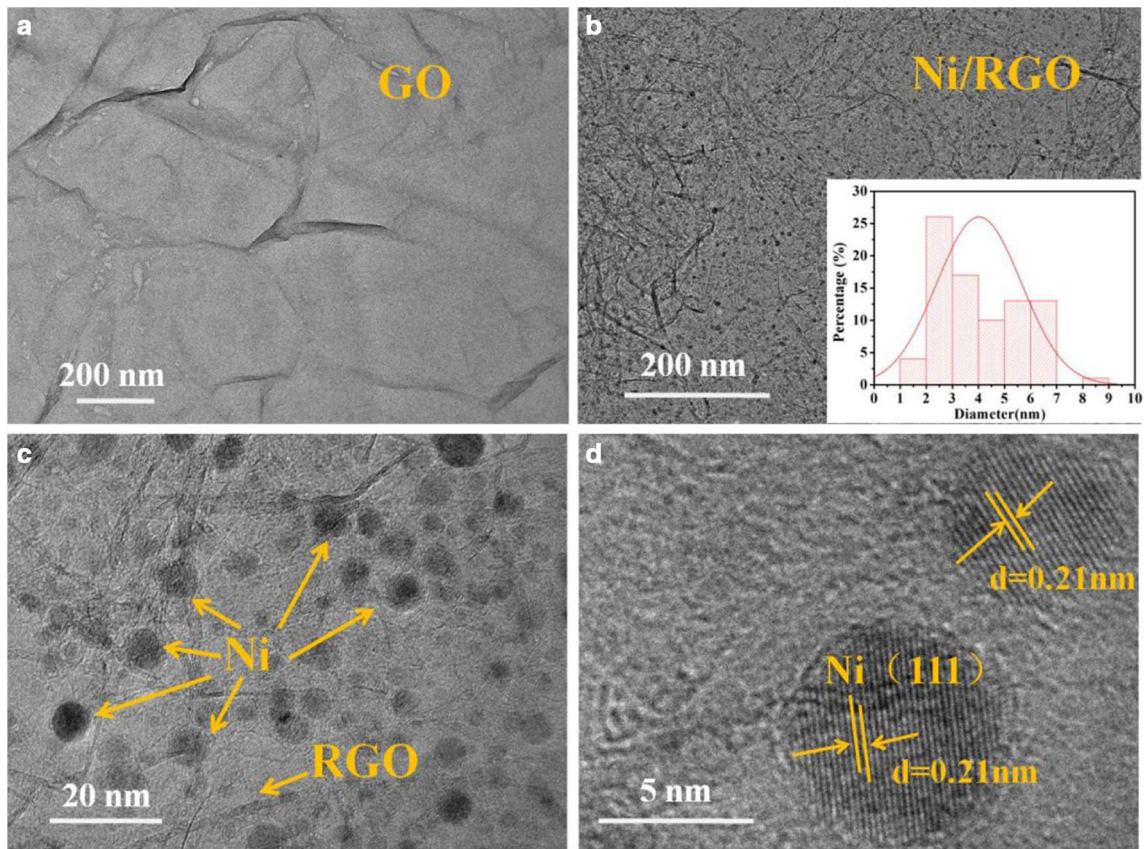


Fig. 2 Low-magnification and high-magnification TEM images of the as-prepared GO (a) and Ni/RGO nanohybrids (b, c, d)

Fig. 3 XPS spectra of a C1s, b Ni2p, and c O1s of Ni/RGO nanocomposite

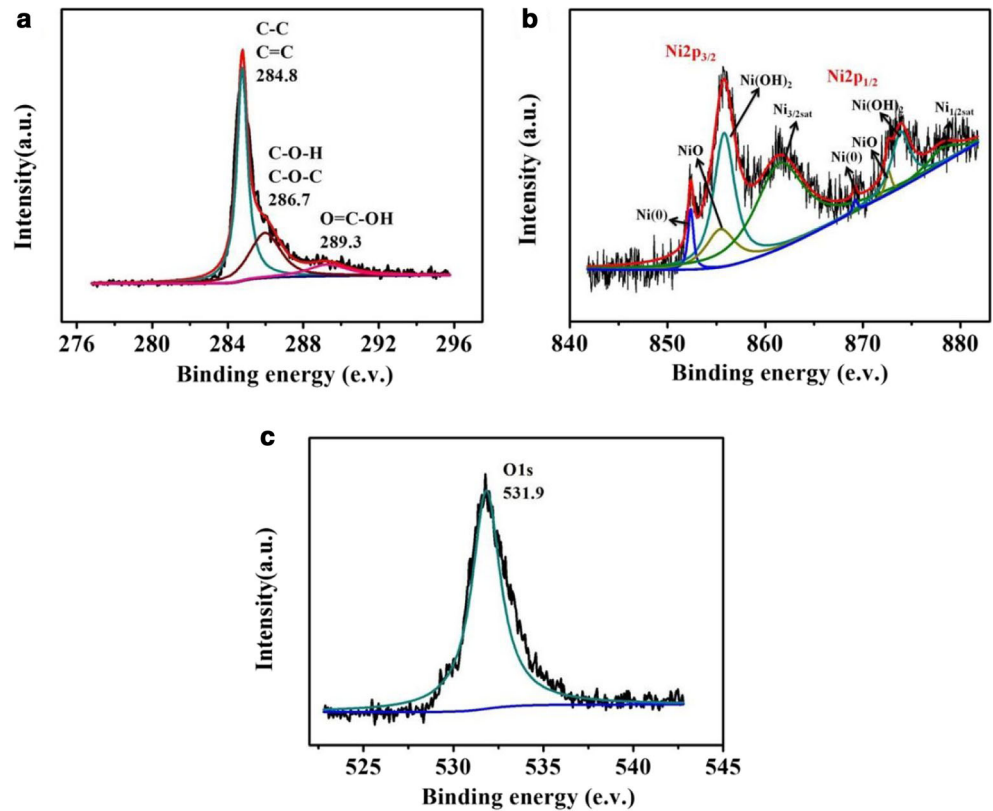
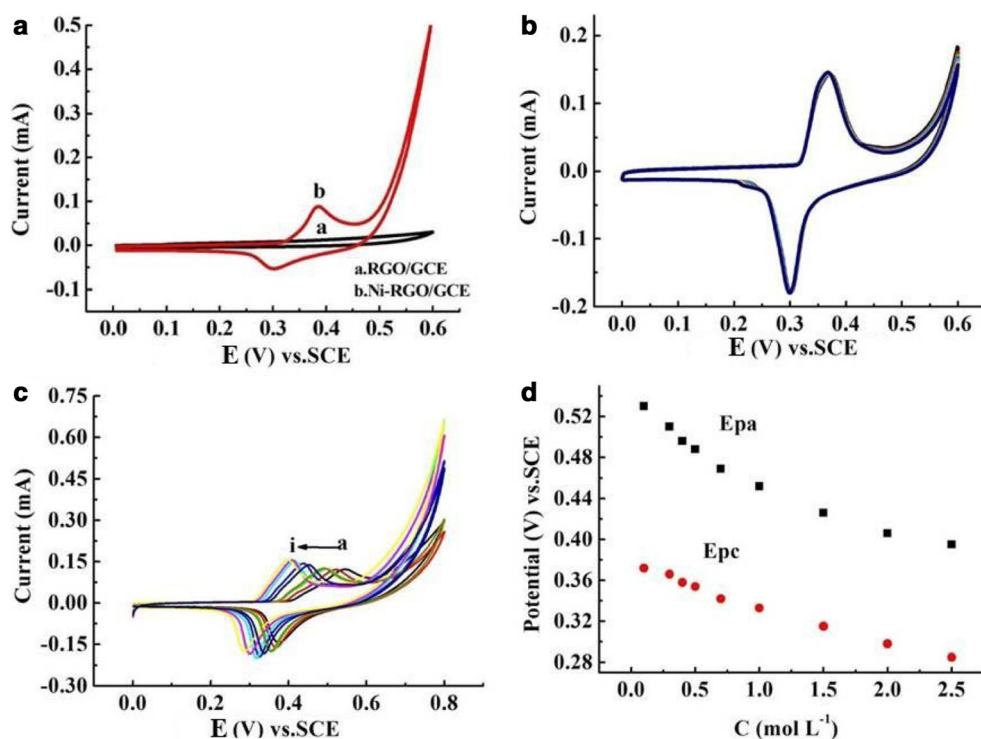
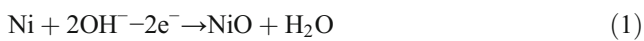


Fig. 4 **a** CVs acquired on RGO/GCE (a) and Ni/RGO/GCE (b) in 1.0 M NaOH solution; **b** CVs of Ni/RGO/GCE in 1.0 M NaOH solution at 30 days, scan rate 50 mV s^{-1} . **c** CVs obtained at Ni/RGO/GCE containing NaOH of 0.1, 0.3, 0.4, 0.5, 0.7, 1.0, 1.5, 2.0, and 2.5 mol L^{-1} ; **d** the plot of redox potentials vs concentrations of NaOH; scan rate 50 mV s^{-1}



the metal Ni(0) could be transformed into Ni(OH)₂ or NiO in the alkaline medium at the onset of the potential scan (0 V).



or



The Ni(OH)₂ and NiO were further oxidized into NiOOH as potential shifted to the positive direction. The possible mechanism involving the direct electrochemical process for Ni/RGO/GCE can be expressed as follows:



or



In addition, Fig. 4b reveals that the stability of the Ni/RGO/GCE was also examined after activation by recording 20 consecutive cyclic voltammogram curves (CVs) for 30 days. No obvious peak current change is found, implying that the modified Ni/RGO is very stable on the surface of the GC electrode.

The influence of NaOH concentration on the electrochemical behavior of Ni/RGO/GCE was investigated, as shown in Fig. 4c, d. In Fig. 4c, it can be seen that with the concentration of NaOH increasing from 0.10 to 2.5 M, both oxidation peak potential and reduction peak potential take place, shifting negatively. Figure 4d clearly indicates that the situations of those

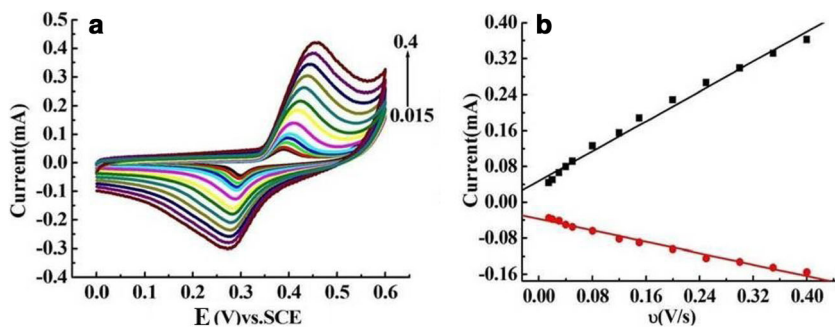
redox peak potentials vary with the change of the concentration of NaOH. Based on laws of chemical thermodynamics, the more negative the oxidation potential, the greater the tendency of the reduced form to be oxidized. Therefore, with an increase in the concentration of NaOH, the oxidation potential of Ni(OH)₂ or NiO becomes more negative, which is consistent with the conclusion induced by the Nernst equation of $E_{\text{pa, Ni(III)/Ni(II)}} = E_{\text{pa, Ni(III)/Ni(II)}}^0 + 0.059 \lg \left(\frac{[\text{Ni(OH)}_3]}{[\text{OH}^-][\text{Ni(OH)}_2]} \right) = E_{\text{pa, Ni(III)/Ni(II)}}^0 - 0.059 \lg [\text{OH}^-]$, corresponding to above-mentioned Eqs. (3) and (4) (activity of both Ni(OH)₃ and Ni(OH)₂ being equal to 1). Meanwhile, the oxidation peak current also increased, with the oxidation potential shifting negatively. In a similar way, based on the above-mentioned Eq. (1) or (2), the Nernst equation of the Ni(0) to be oxidized into Ni(OH)₂ could be expressed as follows:

$$\begin{aligned} E_{\text{Ni(II)/Ni}} &= E_{\text{Ni(II)/Ni}}^0 + 0.059 \lg \left(\frac{[\text{Ni(OH)}_2]}{[\text{OH}^-]^2} \right) \\ &= E_{\text{pa, Ni(II)/Ni}}^0 - 0.059 \lg [\text{OH}^-]^2 \end{aligned} \quad (5)$$

Thus, it can be seen that the $E_{\text{Ni(II)/Ni}}$ also negatively shifts with the increase in the NaOH concentration. The result shows that OH⁻ ion is kinetically involved in the process of electrooxidation reaction of Ni(0). It was that the OH⁻ ions in solution promoted the oxidation of Ni(0) into Ni(II) and Ni(III).

In order to further figure out the electrochemical process of Ni/RGO, the CVs of Ni/RGO/GCE were recorded in 1.0 M NaOH solution at different scan rates, as shown in Fig. 5. It is obvious in Fig. 5a that both redox peaks were enhanced with

Fig. 5 **a** CVs of Ni/RGO/GCE in 1.0 M NaOH at different scan rates; **b** plots of current density vs scan rate (v)



the increase of the scan rate. As can be seen in Fig. 5b, the peak current (I_p) was directly proportional to the potential scan rate within 15–400 mV s^{-1} . The linear regression equations were $I_{pa} = 0.8257v + 0.0501$ ($v: \text{V s}^{-1}, R = 0.9937$) and $I_{pc} = -0.3168v + 0.0373$ ($v: \text{V s}^{-1}, R = 0.9920$), indicating that the electron transfer reaction on the Ni/RGO/GCE involves a surface-controlled process.

Figure 6 presents the CVs of Ni/RGO/GCE in 1.0 M NaOH solution in the presence of ethanol. It is obviously observed that the anode peak currents increase with the increase of ethanol concentration, indicating that the reaction is controlled by the ethanol concentration at the electrode surface. Moreover, the anode peak current (i_p) is a linear correlation with ethanol concentration in the range from 0.25 to 3.0 M with a correlation coefficient of 0.9950, further proving that the oxidation process of ethanol is controlled by the diffusion rate of ethanol from the electrolyte to the active sites of the electrode surface [38]. This result also implies that more ethanol molecules are attached onto Ni(III) active sites, showing that the as-prepared Ni/RGO catalyst has better tolerance for product adsorption [46]. Especially, it is found that the onset potentials of Ni/RGO/GCE shift negatively from 0.345 to 0.326 V as the ethanol concentration is increased, indicating that more ethanol is beneficial to accelerate the reaction more easily.

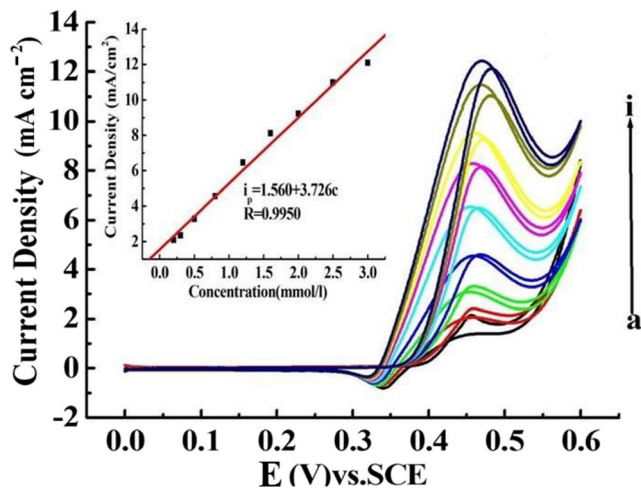


Fig. 6 CVs of Ni/RGO/GCE recorded in 1.0 mol L^{-1} NaOH electrolyte with the addition of various concentrations (0.25–3.0 mol L^{-1}) of ethanol at a scan rate of 50 mV s^{-1} ; inset: i_p vs concentrations of ethanol plots

When the ethanol concentration is 3.0 M, Ni/RGO/GCE in the 1.0 mol L^{-1} NaOH electrolyte delivers the highest peak current density of 12 mA cm^{-2} . When the ethanol concentration exceeds 3.0 M, the peak current no longer increases with increasing ethanol concentration. The reason might be similar to the mechanism study of the ethanol oxidation reaction on the Pd electrode in alkaline media [47], owing to the fact that nickel and palladium belonged to the eighth group transition elements in the same column and had similar chemical properties. As shown in Table 1, the as-prepared Ni/RGO catalyst displays better catalytic performance for electrochemical oxidizing of ethanol than some previously reported nickel-based catalysts [48–50]. Especially, the as-prepared Ni/RGO nanosheet electrode shows a better catalytic role for ethanol oxidation in terms of its relatively low overvoltage and the lower oxidation peak potential value (~ 0.46 V vs. SCE) in comparison to some previous works, such as nickel nanoparticle/graphene aerogel (~ 0.60 V vs. SCE) [37], nano-Ni/graphite electrode (~ 0.60 V vs. Ag/Ag/Cl) [24], nanostructured nickel and nickel-boron tubes (~ 0.60 V vs. Ag/Ag/Cl) [51], FePtSn/C (~ 0.60 V vs. SCE) [22], nickel/multiwalled carbon nanotubes (~ 1.0 V vs. SCE) [52], nickel-dimethylglyoxime complex-modified nickel electrode (~ 0.60 V vs. SCE) [18], and N-doped carbon-encapsulated nickel nanoparticles (~ 0.60 V vs. SCE) [38].

All the obtained experimental results indicate that the Ni/RGO catalyst demonstrates huge potential in DEFCs. It is believed that the improved electrocatalytic activity can be attributed to the synergistic effect of the Ni nanoparticle size and the nanosheet structure of the RGO, which can contribute a large amount of active sites and lead to the high use ratio of Ni.

Chronoamperometry was used to evaluate the stability of the modified electrodes. Figure 7 displays the chronoamperometric response curves of different electrodes in 1.0 M NaOH in the presence (a, c, d) and absence (b) of ethanol. As can be seen in Fig. 7 (curves c and d), no electrochemical responding corresponds to ethanol on RGO/GCE (c) and GCE (d), while curve b corresponds to the electrochemical signal of Ni/RGO/GCE in blank (NaOH) solution, and the current densities of curve b immediately reach a steady state at the initial stage, indicating that the electron transfer reaction involves a surface-controlled process on the Ni/RGO/GCE electrode as described above. Moreover, the current density of the Ni/RGO/GCE is higher than

Table 1 Comparative electrocatalytic performance of various Ni-based catalysts for ethanol oxidation in alkaline solution

Catalysts	Peak current density (mA cm ⁻²)	Ethanol concentration (M)	Reference electrode	Ref.
Ni particles	2.0	1.0	Hg/HgO	49
Ni hollow spheres	17	1.0	Hg/HgO	49
Carbon nanotubes–Ni	0.5	0.2	Ag/AgCl	50
Ni-CMs/WGE	0.1	0.1	Hg/HgO	51
Ni/RGO nanosheets	4.8	1.0	SCE	This work
Ni/RGO nanosheets	12	3.0	SCE	This work

those of the RGO/GCE (Fig. 7, curve c) and GCE (Fig. 7, curve d) in 1.0 M NaOH solution containing 1.0 M ethanol. This implies that the electrocatalytic activity of the Ni/RGO/GCE is improved. Besides, the polarization currents on the Ni/RGO/GC-modified electrode decrease within 300 s and then decay quite slowly to approach a limiting current (up to 1000 s). That initial current rapid decrease can probably be attributed to the formation of the intermediate species during ethanol oxidation reaction [53]. In the inset in Fig. 7, the plot of net current (i) versus the minus square roots of time ($t^{1/2}$) is a linear dependency that was consistent with the Cottrell equation [54], indicating that the electrocatalytic oxidation of ethanol is ostensibly controlled by diffusion.

The oxidation peak of ethanol in negative-going sweep

In the CVs of electrocatalytic oxidation of ethanol (as shown in Fig. 8 (curves a and b)), it is clearly seen that the oxidation peak can appear not only in the positive-going scan but also in

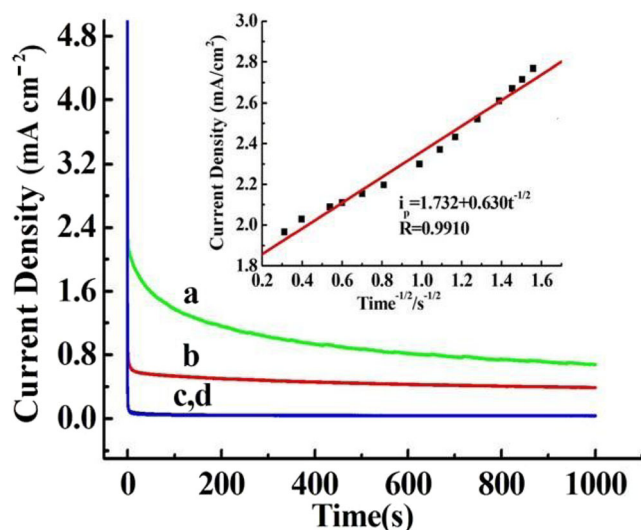


Fig. 7 Chronoamperograms obtained at Ni/RGO/GCE (a), RGO/GCE (c), and GCE (d) in 1.0 M NaOH in the presence and absence (Ni/RGO/GCE, b) of 1.0 mol L⁻¹ ethanol; inset: dependency of transient current on $t^{1/2}$ obtained from curve a; applying potential 0.5 V; sweeping rate 50 mV s⁻¹

the negative-going scan. This interesting phenomenon is greatly different from conventional CVs of reversible systems and irreversible systems. In fact, like ethanol, such as methanol, ethylene glycol, and glycerol as well as aldehyde, etc., their cyclic voltammograms also show similar oxidation peaks during negative-going sweep [45, 46, 55].

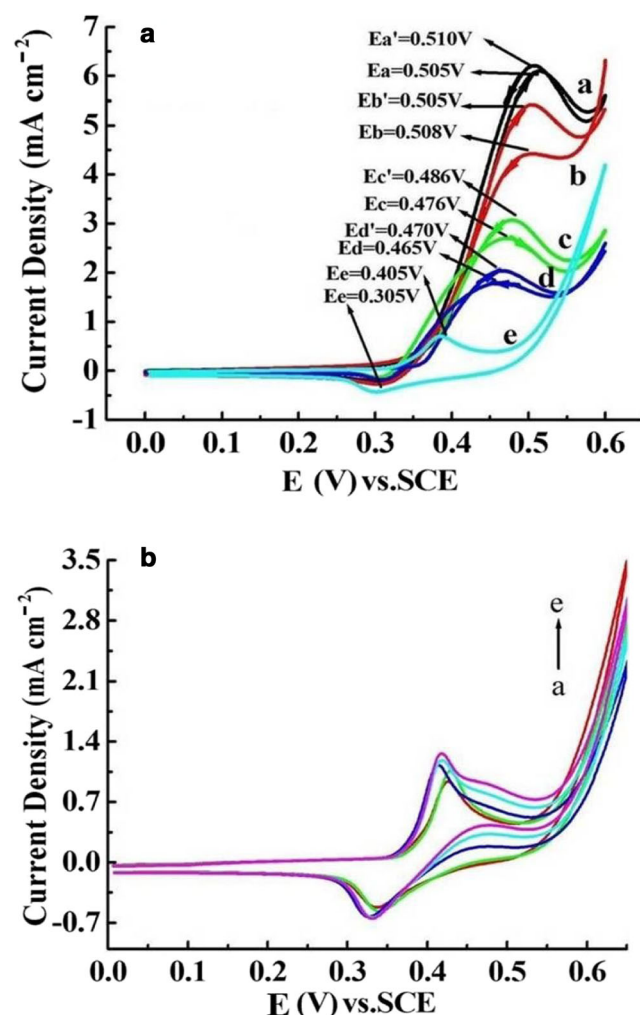


Fig. 8 The CVs of 1.0 mol L⁻¹ ethanol (a, b), 1.0 mol L⁻¹ acetaldehyde (c, d), and supporting electrolyte (e) at Ni/RGO/GCE as well as those of RGO/GCE in the presence (f) and absence (g) of 1.0 mol L⁻¹ ethanol; a, b initial potential 0 V; b, d initial potential 0.6 V; supporting electrolyte 1.0 mol L⁻¹ NaOH; scan rate 50 mV s⁻¹

To date, numerous reports on the researches of the electrocatalytic oxidation mechanism for ethanol in alkaline media have been reported [23, 24, 35, 47]. Among these, Liang et al. [47] proceeded to relatively detail explanations for the electrocatalytic oxidation mechanisms of ethanol. They believed that the acetaldehyde and acetate were active intermediate and final products of ethanol oxidation, respectively. So, they claimed that the oxidation peak in negative-going scan could be ascribed to the reduction of the catalyst oxidation state. To our knowledge, in addition to this work, little study has been carried out to investigate the real reason for this phenomenon. Thus, figuring out the emerging cause of the ethanol oxidation peak in the negative-going sweep is of very important scientific significance. Based on our following study using the CV technique, we believe that these above explanations are not completely convincing.

In order to figure out the causes of the ethanol oxidation peak that appeared in the negative-going scan and eliminate the impact of a one-way sweep curve of the positive-going scan on that of the negative-going scan, the CVs of ethanol oxidation are obtained by adopting a contrary potential scanning mode, as shown in Fig. 8a (curve b). Due to the fact that only the ethanol in the solution can be oxidized and the oxidation peak potential (0.505 V) of the negative-going scan (on curve b) is almost identical (0.508 V) to that of the positive-going scan, it can be concluded that the oxidation peak of the negative-going scan that emerged on curve b (potential scanning direction from 0.6 V of the initial potential to 0 V of the terminal potential) should be ascribed to the oxidation of ethanol.

Comparing curve a with curve b, it can be found that although the sizes of ethanol oxidation peak currents are not the same, the oxidation peak potential (0.510 V) of the negative-going scan that emerged on curve a is also almost identical to that (0.505 V) of its positive-going scan, which is similar to that of curve b. Therefore, the negative-going scan oxidation peak on curve a, like the negative-going scan oxidation peak on curve b, should positively be the oxidation peak of ethanol, rather than the oxidation peak formed by reduction of the catalyst oxidation state as explained by literature. The reason may be that with a high concentration of ethanol, it is difficult to form a stable concentration polarization diffusion layer between the electrode surface and the bulk solution.

In addition, because the oxidation peak potentials of curves a and b in the positive- and negative-going scans are almost the same, this shows that the same oxidation product should be obtained in electrocatalytic oxidation of ethanol under such conditions. This is in view of the fact that the acetaldehyde formed by ethanol oxidation is very easily further oxidized into acetic acid, and meanwhile showing that the oxidation peaks that emerged by the negative-going scan on curves a and b are still the oxidation peaks of ethanol rather than that of acetaldehyde.

In order to distinguish the oxidation peak of ethanol and acetaldehyde, the CVs of acetaldehyde, like ethanol, are

recorded in Fig. 8 (curves c and d) for different potential scanning modes. Similarly, the oxidation peak potentials of acetaldehyde on CVs of curves c and d are completely lower than those of ethanol (curves a and b), indicating that acetaldehyde is easier to be oxidized than ethanol; this is consistent with the acknowledged fact. Based on this point, the oxidation peaks that emerged on CVs of curves a and b by the negative-going scan are indeed the oxidation peak of ethanol rather than that of acetaldehyde. Furthermore, it is found that whether the initial scanning potential is 0 V or 0.6 V, the oxidation peaks that emerge on CVs of curve c and curve d no matter whether positive- or negative-going are also almost the same peak potentials. This means that acetaldehyde, like ethanol, can be not only oxidized in the forward scan but also oxidized in the reverse scan.

Based on the above CV tests, the reasons why ethanol can be also oxidized in the negative-going scan may be related to the following factors:

(I) The influence of ethanol concentration

Ethanol on the electrode surface can be quickly oxidized when the scanning potential arrived at 0.505 V in the positive-going scan (see curve a in Fig. 8a). As a result, a maximum of peak current for oxidation of ethanol is obtained. When the scanning potential exceeds 0.505 V, the oxidation peak current is rapidly decreased accompanied by the increase in scanning potential and the diminishing ethanol concentration on the electrode surface. Ultimately, the limiting diffusion current of ethanol is attained at about 0.57 V on curve a in Fig. 8a due to the diffusion equilibrium of ethanol on the electrode surface.

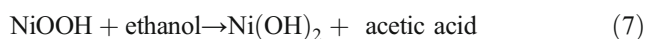
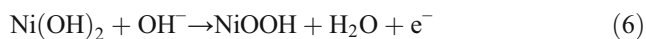
Based on the literature [17], with glucose, concentration 1 mM, containing both alcoholic hydroxyl group and aldehyde group, on the nano-Ni-based electrode, similar to Ni/RGO/GCE in this paper, the oxidation peaks do not emerge on its CVs in the negative-going scan. However, the oxidation peaks can appear on CVs of 1 M of the ethanol and acetaldehyde in the negative-going scan, obviously showing that this is related to the concentration of ethanol. Because it is difficult to form a stable concentration polarization diffusion layer between the electrode surface and bulk solution for a high ethanol concentration in solution, it can again quickly spread to the surface of the electrode and is rapidly oxidized in the negative-going scan, so that the negative-going scan oxidation peak (0.510 V) of ethanol can be detected on curve a in Fig. 8.

In order to verify the effect of ethanol concentration on the oxidation peak of the negative-going scan, the obtained CVs of ethanol within the concentration range of 0.005–0.07 M are displayed in Fig. 8b. As can be clearly seen, the oxidation peak does not appear on the reverse scan, which may be due to the fact that low ethanol concentration in solution easily results in a stable concentration polarization diffusion layer at the working electrode/electrolyte interface. Therefore,

according to the results of Fig. 8, it can be deduced that a high concentration of ethanol in bulk solution plays a great role on the appearance of the ethanol oxidation peak that emerged on the CVs of curve a (Fig. 6) in the reverse scan. This is because the high concentration of ethanol makes it difficult to form a concentration polarization between the electrode surface and the bulk solution.

(II) The effect of the autocatalytic oxidation process at Ni/RGO/GCE

The CVs of Ni/RGO/GCE in 1.0 M NaOH solution in the absence and presence of 1.0 M ethanol are shown in Fig. 8a (curves a, b, and e). In 1.0 M NaOH blank solution (curve e), a pair of well-defined redox peaks at about 0.405 V and 0.305 V is observed, which can be ascribed to the Ni(OH)₂/NiOOH transformation on the surface of Ni/RGO/GCE [56]. After ethanol is added to 1.0 M NaOH solution (curves a and b), a significant increase in the anodic current density at the Ni/RGO/GCE is detected, indicating that the Ni/RGO can greatly promote the oxidation of ethanol. According to some literatures [35, 47] and the above CV tests, the mechanism of ethanol electrochemical oxidation by the Ni(III)/(II) redox couple can be expressed as follows:



Ethanol is oxidized by a chemical reaction with NiOOH species generated by electrochemical oxidation reaction of Ni(OH)₂ on the electrode surface, which decreases the amount of the NiOOH species on the electrode surface, resulting in a decrease in the extent of the electroreduction reaction of the NiOOH species. As a result, as can be seen in Fig. 8a (curve a), the change in concentrations of Ni(II) and Ni(III) species causes the increase of the anodic peak current and the obvious decrease of the cathodic peak current in comparison with those in the absence of ethanol (Fig. 8a (curve e)).

For example, as can be seen in curve a in Fig. 8a, the reverse scan oxidation peak potential of ethanol is about 0.510 V, which is positive than the oxidation peak potential (0.405 V) of transformation of Ni(OH)₂ to NiOOH at the Ni/RGO/GCE surface. Therefore, despite the potential negative scanning, all the Ni(OH)₂ at the Ni/RGO/GCE surface will still be oxidized to NiOOH at about 0.51 V through the electrode reaction. Thus, it is obvious that there are an electrode reaction (*E*) (Eq. 6) and a catalytic chemical reaction (*C*) (Eq. 7), which take place simultaneously at overlapping potential values, corresponding to the oxidation of ethanol and the formation of NiOOH. Furthermore, a high concentration of ethanol diffuses to the electrode surface and is again oxidized by the NiOOH species in the negative-going scan. Especially, the NiOOH species can be regenerated by an electrochemical reaction (*E*) in the negative-going scan,

displaying an autocatalytic process. Consequently, this autocatalytic process and high concentration of ethanol invoke the emergence of an oxidation peak of ethanol on the CVs in the negative-going scan.

Conclusions

In summary, nickel nanoparticles anchored on reduced graphene oxide nanosheets have been fabricated via a facile wet-chemical method. The achieved Ni/RGO catalyst was characterized via various techniques including FE-SEM, EDX, TEM, XRD, XPS, and Raman spectroscopy. It is found that many highly dispersed Ni nanoparticles with a particle size of 4–8 nm are anchored on the RGO nanosheets. Moreover, the electrocatalytic properties of the Ni/RGO catalyst have been evaluated for ethanol oxidation in the alkaline media. It was proved that Ni/RGO/GCE can present an excellent catalytic activity and stability toward ethanol oxidation in terms of the low peak potential value, the low reduction of its overvoltage, and satisfactory peak current density. All the obtained experimental results indicate that the Ni/RGO catalyst demonstrates huge potential in DEFCs. The excellent electrocatalytic properties could be ascribed to the synergistic effect of Ni spherical nanoparticles and RGO nanosheets, which can lead to the high use ratio of Ni. Especially, for the first time, it is proposed that the anodic peak that emerged in the potential negative-going sweep may be attributed to the oxidation of ethanol, which is different from other reasons reported in related literatures. Also, it is believed that an autocatalytic process at Ni/RGO/GCE and high concentration of ethanol invoke the emergence of the oxidation peak of ethanol on the CVs in the negative-going scan. These above findings are conducive to figure out the mechanism of nickel-based catalysts for ethanol electrooxidation reaction in the fuel cells in future related researches.

Funding The authors thank the Natural Science Foundation of China (No. 51604098), Program for Science & Technology Innovation Talents in Universities of Henan Province (No. 17HASTIT030), and Henan Key Science and Technology Program of China (No. 132102210256) for the financial support.

References

1. Zakaria Z, Kamarudin SK, Timmiati SN (2016) Membranes for direct ethanol fuel cells: an overview. *Appl Energy* 163:334–342
2. Akhairi MAF, Kamarudin SK (2016) Catalysts in direct ethanol fuel cell (DEFC): an overview. *Int J Hydrog Energy* 41:4214–4228
3. Li YS, Zhao TS, Liang ZX (2009) Performance of alkaline electrolyte-membrane-based direct ethanol fuel cells. *J Power Sources* 187:387–392
4. Antolini E (2007) Catalysts for direct ethanol fuel cells. *J Power Sources* 170:1–12

5. Peled E, Livshits V, Duvdevani T (2002) High-power direct ethylene glycol fuel cell (DEGFC) based on nanoporous proton-conducting membrane (NP-PCM). *J Power Sources* 106:245–248
6. Wang A-J, Ju K-J, Zhang Q-L, Song P, Wei J, Feng J-J (2016) Folic acid bio-inspired route for facile synthesis of AuPt nanodendrites as enhanced electrocatalysts for methanol and ethanol oxidation reactions. *J Power Sources* 326:227–234
7. Yang Z-Z, Liu L, Wang A-J, Yuan J, Feng J-J, Xu Q-Q (2017) Simple wet-chemical strategy for large-scaled synthesis of snowflake-like PdAu alloy nanostructures as effective electrocatalysts of ethanol and ethylene glycol oxidation. *Int J Hydrog Energy* 42:2034–2044
8. Badwal SPS, Giddey S, Kulkarni A, Goel J, Basu S (2015) Direct ethanol fuel cells for transport and stationary applications – a comprehensive review. *Appl Energy* 145:80–103
9. Guo X, Deng H, Zhou H, Fan T, Gao Z (2015) Detection of glucose with a lamellar-ridge architected gold modified electrode. *Sensors Actuators B Chem* 206:721–727
10. Gharibi H, Sadeghi S, Golmohammadi F (2016) Electrooxidation of ethanol on highly active and stable carbon supported PtSnO₂ and its application in passive direct ethanol fuel cell: effect of tin oxide synthesis method. *Electrochim Acta* 190:1100–1112
11. Mukherjee P, Bagchi J, Dutta S, Bhattacharya SK (2015) The nickel supported platinum catalyst for anodic oxidation of ethanol in alkaline medium. *Appl Catal A Gen* 506:220–227
12. Figueiredo MC, Solla-Gullón J, Vidal-Iglesias FJ, Nisula M, Feliu JM, Kallio T (2015) Carbon-supported shape-controlled Pt nanoparticle electrocatalysts for direct alcohol fuel cells. *Electrochem Commun* 55:47–50
13. Zignani SC, Baglio V, Sebastián D, Siracusano S, Aricò AS (2016) Enhancing ethanol oxidation rate at PtRu electro-catalysts using metal-oxide additives. *Electrochim Acta* 191:183–191
14. Mao H, Huang T, Yu A (2016) Surface noble metal modified PdM/C (M = Ru, Pt, Au) as anode catalysts for direct ethanol fuel cells. *J Alloys Compd* 676:390–396
15. Liu L, Chen L-X, Wang A-J, Yuan J, Shen L, Feng J-J (2016) Hydrogen bubbles template-directed synthesis of self-supported AuPt nanowire networks for improved ethanol oxidation and oxygen reduction reactions. *Int J Hydrog Energy* 41:8871–8880
16. Hu X, Lin C, Wei L, Hong C, Zhang Y, Zhuang N (2016) High electrocatalytic performance of graphene nanoribbon supported PtAu nanoalloy for direct ethanol fuel cell and theoretical analysis of anti-CO poisoning. *Electrochim Acta* 187:560–566
17. Lu L-M, Zhang L, Qu F-L, Lu H-X, Zhang X-B, Wu Z-S, Huan SY, Wang QA, Shen GL, Yu RQ (2009) A nano-Ni based ultrasensitive nonenzymatic electrochemical sensor for glucose: enhancing sensitivity through a nanowire array strategy. *Biosens Bioelectron* 25: 218–223
18. Golikand AN, Asgari M, Maragheh MG, Shahrokhian S (2006) Methanol electrooxidation on a nickel electrode modified by nickel–dimethylglyoxime complex formed by electrochemical synthesis. *J Electroanal Chem* 588:155–160
19. Golikand AN, Shahrokhian S, Asgari M, Ghannadi Maragheh M, Irannejad L, Khanchi A (2005) Electrocatalytic oxidation of methanol on a nickel electrode modified by nickel dimethylglyoxime complex in alkaline medium. *J Power Sources* 144:21–27
20. Fleischmann M, Korinek K, Pletcher D (1971) The oxidation of organic compounds at a nickel anode in alkaline solution. *J Electroanal Chem Interfacial Electrochem* 31:39–49
21. Antolini E, Gonzalez ER (2010) Alkaline direct alcohol fuel cells. *J Power Sources* 195:3431–3450
22. Wang Z, Fan H, Liang H, Ma J, Li S, Song Y, Wang R (2017) Microfluidic synthesis and characterization of FePtSn/C catalysts with enhanced electro-catalytic performance for direct methanol fuel cells. *Electrochim Acta* 230:245–254
23. Cuña A, Reyes Plascencia C, da Silva EL, Marcuzzo J, Khan S, Tancredi N, Baldan MR, de Fraga Malfatti C (2017) Electrochemical and spectroelectrochemical analyses of hydrothermal carbon supported nickel electrocatalyst for ethanol electro-oxidation in alkaline medium. *Appl Catal B Environ* 202:95–103
24. Soliman AB, Abdel-Samad HS, Abdel Rehim SS, Ahmed MA, Hassan HH (2016) High performance nano-Ni/graphite electrode for electro-oxidation in direct alkaline ethanol fuel cells. *J Power Sources* 325:653–663
25. Qi J, Benipal N, Liang C, Li W (2016) PdAg/CNT catalyzed alcohol oxidation reaction for high-performance anion exchange membrane direct alcohol fuel cell (alcohol = methanol, ethanol, ethylene glycol and glycerol). *Appl Catal B Environ* 199:494–503
26. Geraldine AN, Furtunato da Silva D, Martins da Silva JC, Antonio de Sá O, Spinacé EV, Neto AO, Coelho dos Santos M (2015) Palladium and palladium–tin supported on multi wall carbon nanotubes or carbon for alkaline direct ethanol fuel cell. *J Power Sources* 275:189–199
27. Zhang Y, Zhou E, Li Y, He X (2015) A novel nonenzymatic glucose sensor based on magnetic copper ferrite immobilized on multiwalled carbon nanotubes. *Anal Methods* 7:2360–2366
28. Chen D, Tang L, Li J (2010) Graphene-based materials in electrochemistry. *Chem Soc Rev* 39:3157–3180
29. Shanguan E, Guo L, Li F, Wang Q, Li J, Li Q, Chang Z, Yuan XZ (2016) FeS anchored reduced graphene oxide nanosheets as advanced anode material with superior high-rate performance for alkaline secondary batteries. *J Power Sources* 327:187–195
30. Niu L, Wang J, Hong W, Sun J, Fan Z, Ye X, Wang H, Yang S (2014) Solvothermal synthesis of Ni/reduced graphene oxide composites as electrode material for supercapacitors. *Electrochim Acta* 123:560–568
31. Lo Faro M, Reis RM, Saglietti GGA, Zignani SC, Trocino S, Frontera P, Antonucci PL, Ticianelli EA, Aricò AS (2015) Investigation of Ni-based alloy/CGO electro-catalysts as protective layer for a solid oxide fuel cell anode fed with ethanol. *J Appl Electrochem* 45:647–656
32. Ghanem MA, Al-Mayouf AM, Singh JP, Abiti T, Marken F (2015) Mesoporous nickel/nickel hydroxide catalyst using liquid crystal template for ethanol oxidation in alkaline solution. *J Electrochem Soc* 162:H453–H459
33. Kakaei K, Marzang K (2016) One – step synthesis of nitrogen doped reduced graphene oxide with NiCo nanoparticles for ethanol oxidation in alkaline media. *J Colloid Interface Sci* 462:148–153
34. Hassaninejad-Darzi SK, Gholami-Esfidvajani M (2016) Electrocatalytic oxidation of ethanol using modified nickel phosphate nanoparticles and multi-walled carbon nanotubes paste electrode in alkaline media for fuel cell. *Int J Hydrog Energy* 41: 20085–20099
35. Barbosa AFB, Oliveira VL, van Drunen J, Tremiliosi-Filho G (2015) Ethanol electro-oxidation reaction using a polycrystalline nickel electrode in alkaline media: temperature influence and reaction mechanism. *J Electroanal Chem* 746:31–38
36. Liu Z, Li Z, Wang F, Liu J, Ji J, Wang J, Wang W, Qin S, Zhang L (2011) Synthesis of multi-walled carbon nanotube supported nickel catalysts by hydrazine reduction and their electrocatalytic activity on ethanol electro-oxidation. *Mater Lett* 65:3396–3398
37. Ren L, Hui KS, Hui KN (2013) Self-assembled free-standing three-dimensional nickel nanoparticle/graphene aerogel for direct ethanol fuel cells. *J Mater Chem A* 1:5689–5694
38. Shi W, Wang Q, Qin F, Yu J, Jia M, Gao H, Zhang Y, Zhao Y, Li G (2017) N-doped carbon encapsulated nickel nanoparticles: rational fabrication and ultra-high performance for ethanol oxidation. *Electrochim Acta* 232:332–338
39. Deng Z, Yi Q, Zhang Y, Nie H (2017) NiCo/C-N/CNT composite catalysts for electro-catalytic oxidation of methanol and ethanol. *J Electroanal Chem* 803:95–103

40. Hummers WS, Offeman RE (1958) Preparation of graphitic oxide. *J Am Chem Soc* 80:1339
41. Li N, Cao M, Wu Q, Hu C (2012) A facile one-step method to produce Ni/graphene nanocomposites and their application to the thermal decomposition of ammonium perchlorate. *CrystEngComm*. 14:428–434
42. Zhong S, Tian R, Zhang N, Liang Q, Jiang W, Wang T (2016) Design and synthesis of magnetically separable photocatalyst incorporated with urchin-like Ni as magnetic component to enhance photocatalytic performance. *J Photochem Photobiol A Chem* 330: 126–133
43. Tian Y, Liu Y, Pang F, Wang F, Zhang X (2015) Green synthesis of nanostructured Ni-reduced graphene oxide hybrids and their application for catalytic reduction of 4-nitrophenol. *Colloids Surf A Physicochem Eng Asp* 464:96–103
44. Geng J, Kuai L, Kan E, Sang Y, Geng B (2016) Hydrothermal synthesis of a rGO nanosheet wrapped NiFe nanoalloy for superior electrocatalytic oxygen evolution reactions. *Chem Eur J* 22: 14480–14483
45. Asgari M, Maragheh MG, Davarkhah R, Lohrasbi E, Golikand AN (2012) Electrocatalytic oxidation of methanol on the nickel–cobalt modified glassy carbon electrode in alkaline medium. *Electrochim Acta* 59:284–289
46. Al-Enizi AM, Ghanem MA, El-Zatahry AA, Al-Deyab SS (2014) Nickel oxide/nitrogen doped carbon nanofibers catalyst for methanol oxidation in alkaline media. *Electrochim Acta* 137:774–780
47. Liang ZX, Zhao TS, Xu JB, Zhu LD (2009) Mechanism study of the ethanol oxidation reaction on palladium in alkaline media. *Electrochim Acta* 54:2203–2208
48. Xu C, Hu Y, Rong J, Jiang SP, Liu Y (2007) Ni hollow spheres as catalysts for methanol and ethanol electrooxidation. *Electrochem Commun* 9:2009–2012
49. Suleimanov NM, Khantimerov SM, Kukovitsky EF, Matukhin VL (2008) Electrooxidation of ethanol on carbon nanotubes–nickel nanoparticles composites in alkaline media. *J Solid State Electrochem* 12:1021–1023
50. Guan-Ping JR, Baron, Lei X, Richard G, Compton (2009) Ultrasonic synthesis of nickel nanostructures on glassy carbon microspheres and their application for ethanol electrooxidation. *J Nanosci Nanotechnol* 9:2719–2725
51. Muench F, Oezaslan M, Rauber M, Kaserer S, Fuchs A, Mankel E, Brötz J, Strasser P, Roth C, Ensinger W (2013) Electroless synthesis of nanostructured nickel and nickel–boron tubes and their performance as unsupported ethanol electrooxidation catalysts. *J Power Sources* 222:243–252
52. Jin G-P, Ding Y-F, Zheng P-P (2007) Electrodeposition of nickel nanoparticles on functional MWCNT surfaces for ethanol oxidation. *J Power Sources* 166:80–86
53. Wang L, Lu X, Ye Y, Sun L, Song Y (2013) Nickel-cobalt nanostructures coated reduced graphene oxide nanocomposite electrode for nonenzymatic glucose biosensing. *Electrochim Acta* 114:484–493
54. Zhang Q-L, Zheng J-N, Xu T-Q, Wang A-J, Wei J, Chen J-R, Feng JJ (2014) Simple one-pot preparation of Pd-on-cu nanocrystals supported on reduced graphene oxide for enhanced ethanol electrooxidation. *Electrochim Acta* 132:551–560
55. Yuan L-S, Zheng Y-X, Jia M-L, Zhang S-J, Wang X-L, Peng C (2015) Nanoporous nickel-copper-phosphorus amorphous alloy film for methanol electro-oxidation in alkaline medium. *Electrochim Acta* 154:54–62
56. Lv J-J, Li S-S, Wang A-J, Mei L-P, Chen J-R, Feng J-J (2014) Monodisperse Au-Pd bimetallic alloyed nanoparticles supported on reduced graphene oxide with enhanced electrocatalytic activity towards oxygen reduction reaction. *Electrochim Acta* 136:521–528

Publisher's note Springer Nature remains neutral with regard to jurisdictional claims in published maps and institutional affiliations.